Modeling of advanced divertor configuration on experimental advanced superconducting tokamak by SOLPS5.0/B2.5-Eirene

H. Si' , H. Y. Guo' , G. S. Xu, B. J. Xiao, Z. P. Luo, Y. Guo, L. Wang, R. Ding, and the EAST Team

Citation: Physics of Plasmas **23**, 032502 (2016); doi: 10.1063/1.4943282
View online: http://dx.doi.org/10.1063/1.4943282
View Table of Contents: http://aip.scitation.org/toc/php/23/3
Published by the American Institute of Physics

Modeling of advanced divertor configuration on experimental advanced superconducting tokamak by SOLPS5.0/B2.5-Eirene

H. Si,[1,a)] H. Y. Guo,[1,2,b)] G. S. Xu,[1] B. J. Xiao,[1] Z. P. Luo,[1] Y. Guo,[1] L. Wang,[1] R. Ding,[1] and the EAST Team[1]
[1]*Institute of Plasma Physics, Chinese Academy of Sciences, Hefei 230031, China*
[2]*General Atomics, P.O. Box 85608, San Diego, California 92186, USA*

(Received 11 October 2015; accepted 23 February 2016; published online 4 March 2016)

Heat exhaust is one of the most challenging issues to be addressed for tokamak magnetic confinement fusion research. Detailed modeling with SOLPS5.0/B2.5-Eirene code package is carried out to examine an alternative advanced divertor configuration, i.e., quasi snowflake (QSF), for long pulse operation in EAST. Comparison is also made with the lower single null (LSN) divertor configuration. SOLPS predicts that the quasi snowflake configuration significantly reduces the peak heat flux at the lower divertor outer target, by a factor of 2–3, owing to the magnetic flux expansion. Furthermore, the density threshold for detachment is much lower for QSF, compared to LSN under the same upstream conditions. This indicates that QSF provides a promising tool for controlling heat flux at divertor target while maintaining a lower separatrix density, which is highly desirable for current drive, thus greatly facilitating long-pulse operation in EAST. © *2016 AIP Publishing LLC*.
[http://dx.doi.org/10.1063/1.4943282]

I. INTRODUCTION

Power exhaust is a key challenge facing high power, long pulse operation for tokamaks. A number of advanced divertor concepts, such as snowflake divertor,[1–8] Super-X divertor,[9–12] X-divertor,[13–15] have been explored as a promising approach towards addressing this critical issue for the next-step fusion development.

The Experimental Advanced Superconducting Tokamak, EAST, with the major radius $R = 1.85$ m, the minor radius $a = 0.45$ m, the plasma current $I_p \leq 1$ MA, and the toroidal field $B_T \leq 3.5$ T, is fully superconducting magnetic confinement facility with ITER-like magnetic field configuration and heating scheme. It is aimed at demonstrating high-power and long-pulse plasma operations with the expected plasma pulse up to 1000 s, thus providing a test bed for addressing some physics and engineering issues for the next-step, high-power and long-pulse fusion devices such as ITER and beyond.[16–23] EAST features a flexible poloidal field control system, accommodating lower single null (LSN), upper single null (USN), and double null (DN) divertor configurations. During the last two EAST experimental campaigns in 2014 and 2015, an alternative advanced divertor configuration, i.e., quasi snowflake (QSF), aka X-divertor, has also been attempted, as shown in Fig. 1.[24]

Modeling with the SOLPS5.0/B2.5-Eirene code package has been carried out to evaluate the performance of QSF and provide guidance to the experiments. This paper assesses the basic features of QSF formed at the lower divertor in EAST, with respect to LSN in EAST, using SOLPS. The rest of the paper is organized as follows. Firstly, Section II describes the key input parameters used in SOLPS modeling. Then, Section III presents the basic divertor plasma behavior for QSF divertor configuration, as predicted by SOLPS, in comparison with LSN under the same upstream plasma condition, followed by a summary.

II. SOLPS MODELLING INPUTS

SOLPS5.0 code package consists of a multi-fluid plasma code B2.5 for ions and electrons at each ionization state and a kinetic Monte-Carlo code Eirene for neutral solver for the plasma edge of tokamaks including the outer core edge, scrape-off layer (SOL), and divertor regions, taking into account the detailed atomic processes, such as collision, ionization, and recombination.[25–30] In the code, the radial-poloidal plasma distributions on a representative poloidal cross-section of EAST are sampled by the computational mesh, as shown in Fig. 2. With respect to EAST LSN divertor configuration (Fig. 2(a), named "DivA"), the connection length in EAST QSF divertor configuration (Fig. 2(b), i.e., "DivB") is increased by ∼30%, and, furthermore, the flux expansion in the lower outer target is increased by a factor ∼4. More detailed parameters for both divertor configurations are listed in Table I.[24]

The power flowing into the edge plasma from the core is given by

$$P_{SOL} = P_{LHW} + P_{OHM} + P_{NBI} - P_{rad}. \quad (1)$$

For both QSF and LSN divertor configurations, the power flux at the core-edge boundary is fixed at $P_{SOL} = 2$ MW, including both ion and electron channels, assuming $P_i = P_e$ at the core-edge boundary. The ion density for core-edge boundary at the outer midplane, n_u, is used as a key control parameter in the simulations to achieve different divertor plasma conditions. Assume n_u has a linear relationship with the line-averaged plasma density $\overline{n_e}$ under a given magnetic configuration,[31] as given by

[a)]Electronic mail: hsi@ipp.cas.cn
[b)]Electronic mail: hyguo@ipp.ac.cn

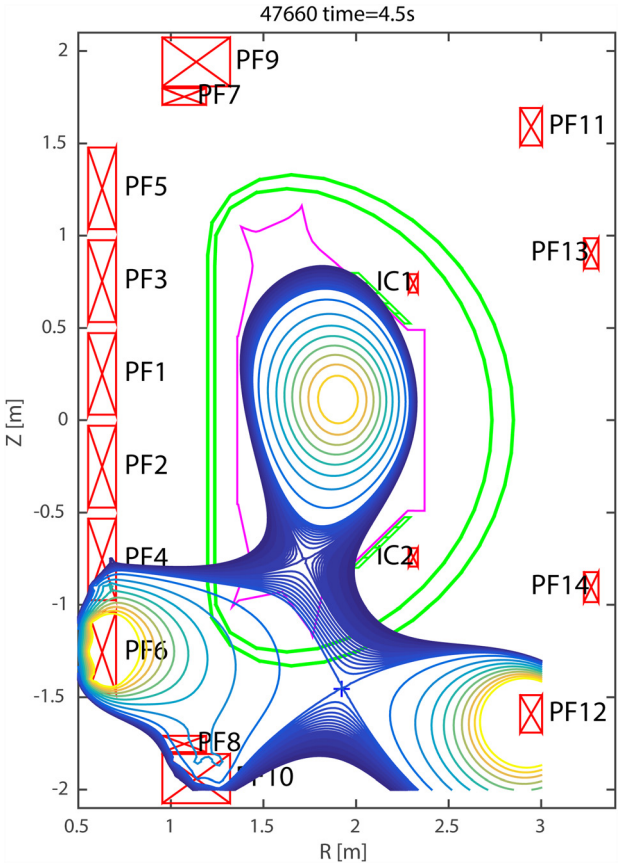

FIG. 1. The EFIT equilibrium of QSF discharge 47660 shot at 4.5 s.

$$n_u = 0.0023\bar{n}_e^{1.08}\kappa^{1.11}B_\phi^{0.78}. \tag{2}$$

The cross-field transport is simply treated as being diffusive, with the particle and heat fluxes given by

$$\Gamma_\perp = D_\perp \frac{dn}{dr}, \tag{3}$$

TABLE I. The poloidal angle of the target and total angel of incidence of the field line for both divertor configurations.

	DivA:LSN	DivB:QSF
Poloidal angle at outer target (deg)	34.28	34.83
Poloidal angle at inner target (deg)	42.32	62.63
Total angel at outer target (deg)	1.17	0.31
Total angel at inner target (deg)	1.23	0.86

$$q_\perp^{cond} = -\kappa_\perp \frac{dkT}{dr} = -n\chi_\perp \frac{dkT}{dr}, \tag{4}$$

assuming that the anomalous particle diffusivity, $D_\perp = 0.5\,\mathrm{m}^2/\mathrm{s}$ and the anomalous ion and electron thermal diffusivity, $\chi_i = \chi_e = \chi_\perp = 1.0\,\mathrm{m}^2/\mathrm{s}$. For simplicity, the cross-field drifts are not included in the simulation. The particle species used in the simulation include deuterium atom D^0, deuterium ion D^{+1}, and electron e. The simple Bohm boundary condition is applied at the divertor target plates, i.e., the ion parallel velocity reaches the ion sound speed[32,33]

$$v_t = c_{st}. \tag{5}$$

In addition, the parallel plasma transport is assumed to be classical but flux limited. When ions hit the wall or the divertor target plates, some of them return as recycling neutrals. The recycling coefficient is set to 100% for deuterium under steady state operating conditions.

III. RESULTS AND DISCUSSIONS

There are three distinct regimes for divertor plasmas, including sheath limited regime, conduction limited regime, and detached plasma regime, which are mainly determined by the classical transport along the magnetic field lines in the SOL.[32]

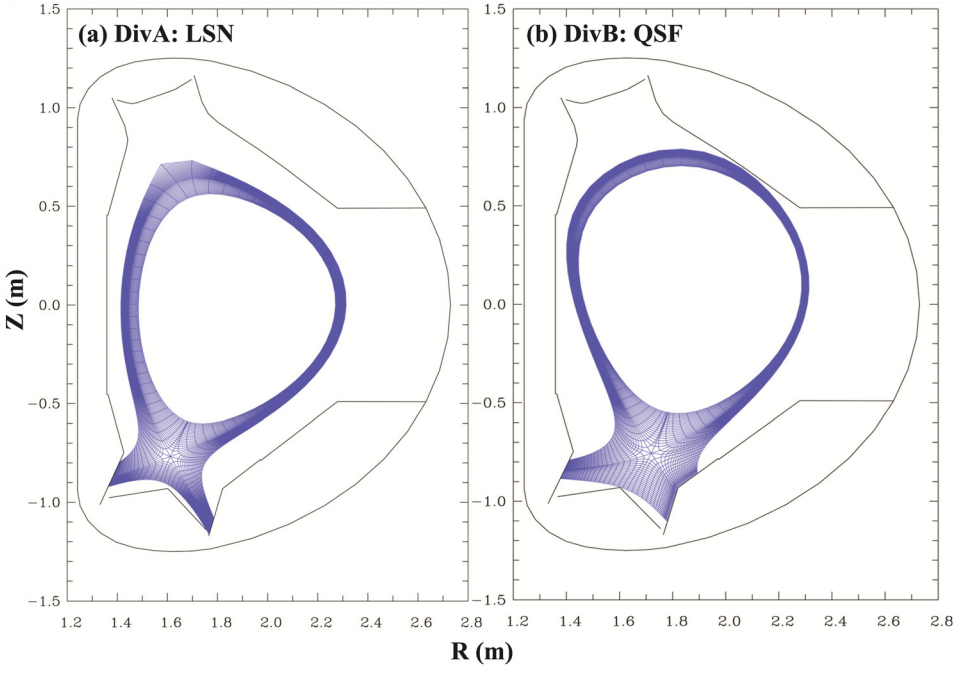

FIG. 2. The computational meshes of both different EAST divertor configurations for SOLPS simulations: (a) LSN (DivA) and (b) QSF (DivB).

In the SOLPS modelling, n_u is varied from 0.1×10^{19} m^{-3} to 1.0×10^{20} m^{-3}. The peak value of electron density, electron temperature, integral particle flux, parallel heat flux to the separatrix of outer midplane, total radiated power, and peak heat flux at the lower outer target for both LSN and QSF divertor configurations are presented as a function of separatrix density at the outer midplane, n_e^{sep}, in Fig. 3. The peak values of electron density for both LSN and QSF increase with increasing n_e^{sep}, as shown in Fig. 3(a). For QSF, the divertor plasma quickly enters into the high recycling regime as n_e^{sep} rises, manifested by a rapid increase in the divertor plasma density for QSF, in contrast to the LSN case, as to be discussed later. As n_e^{sep} further increases, the divertor density starts to rollover for QSF, suggesting that the plasma starts to detach at the target, while the divertor plasma is still in the recycling regime, which is more clear from the rollover in the integral particle flux, as shown in Fig. 3(c). The peak values of electron temperature for both divertor configurations decrease with increasing n_e^{sep}, and the peak electron temperature for QSF is lower than that for LSN at the same n_e^{sep}, as shown in Fig. 3(b). In Fig. 3(d), the parallel heat fluxes for both LSN and QSF divertor configurations are similar. In the simulations only considering deuterium without any other impurities, total radiated power are similar for both LSN and QSF divertor configurations, which is clearly shown in Fig. 3(e). Owing to the greater flux expansion of QSF at the lower outer target caused by smaller incident field line angle, the peak heat flux is much lower than that for LSN under the same n_e^{sep} with the peak value being reduced by a factor of 2–3, even prior to the detachment, as shown in Fig. 3(f).

In the low recycling regime, sheath-limited regime, the plasma is in the SOL with pressure balance between the upstream plasma and the divertor plasma, i.e.,

$$T_u = T_i, \tag{6}$$

and

$$n_u T_u = 2 n_t T_t, \tag{7}$$

where $T = (T_i + T_e)/2$. The divertor plasma density increases linearly with the upstream density at the midplane, Fig. 3(a). Figure 4 shows the profiles of total pressure p and electron temperature T_e for the upstream outer midplane and downstream outer lower target, as well as the heat flux at the lower outer target Q_t, for both LSN and QSF divertor configurations with $n_e^{sep} = 0.35 \times 10^{19}$ m^{-3}. As can be seen, the upstream p and T_e are nearly the same as those at the outer target for both divertor configurations, as expected for the sheath limited regime. As n_e^{sep} increases gradually, the divertor plasma enters from the sheath limited regime to the conduction limited regime, also referred to as high recycling regime. The plasma pressure keeps constant along the field

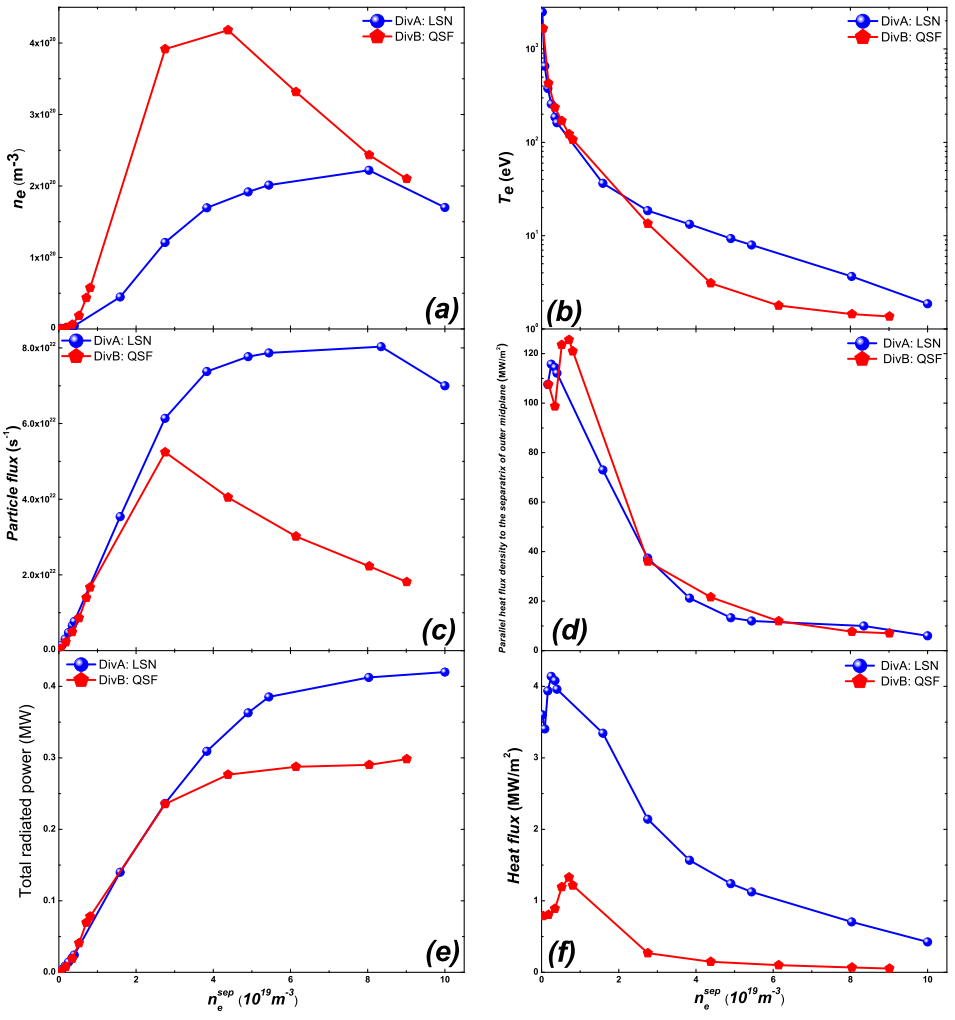

FIG. 3. The peak values of electron density (a), electron temperature (b), particle flux (c), parallel heat flux to the separatrix of outer midplane (d), total radiated power (e), and peak heat flux (f) at lower outer target for both different EAST divertor configurations (DivA and DivB) as a function of n_e^{sep}.

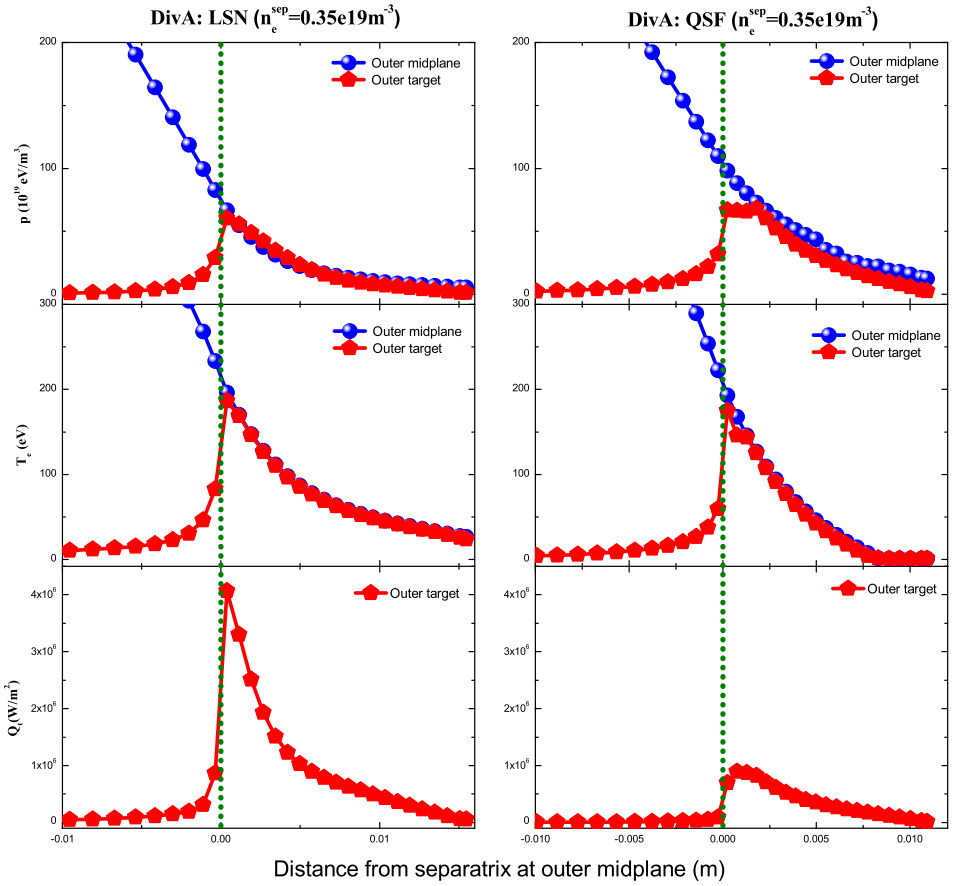

FIG. 4. The radial profiles of total pressure, electron temperature for the upstream and lower outer target, as well as the heat flux at lower outer target, versus the distance from the separatrix, mapped to the outer midplane, for both different EAST LSN and QSF divertor configurations with $n_e^{sep} = 0.35 \times 10^{19}\,\mathrm{m}^{-3}$.

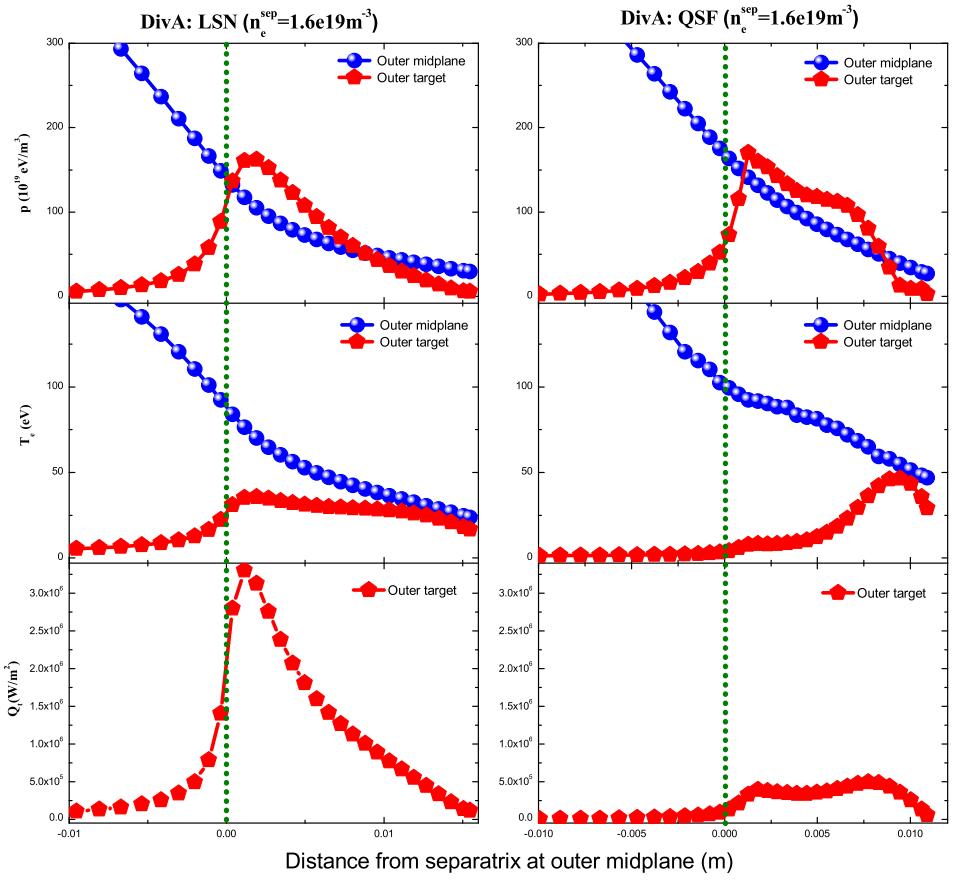

FIG. 5. The radial profiles of total pressure, electron temperature for the upstream and lower outer target, as well as the heat flux at lower outer target, versus the distance from the separatrix, mapped to the outer midplane, for both different EAST LSN and QSF divertor configurations with $n_e^{sep} = 1.6 \times 10^{19}\,\mathrm{m}^{-3}$.

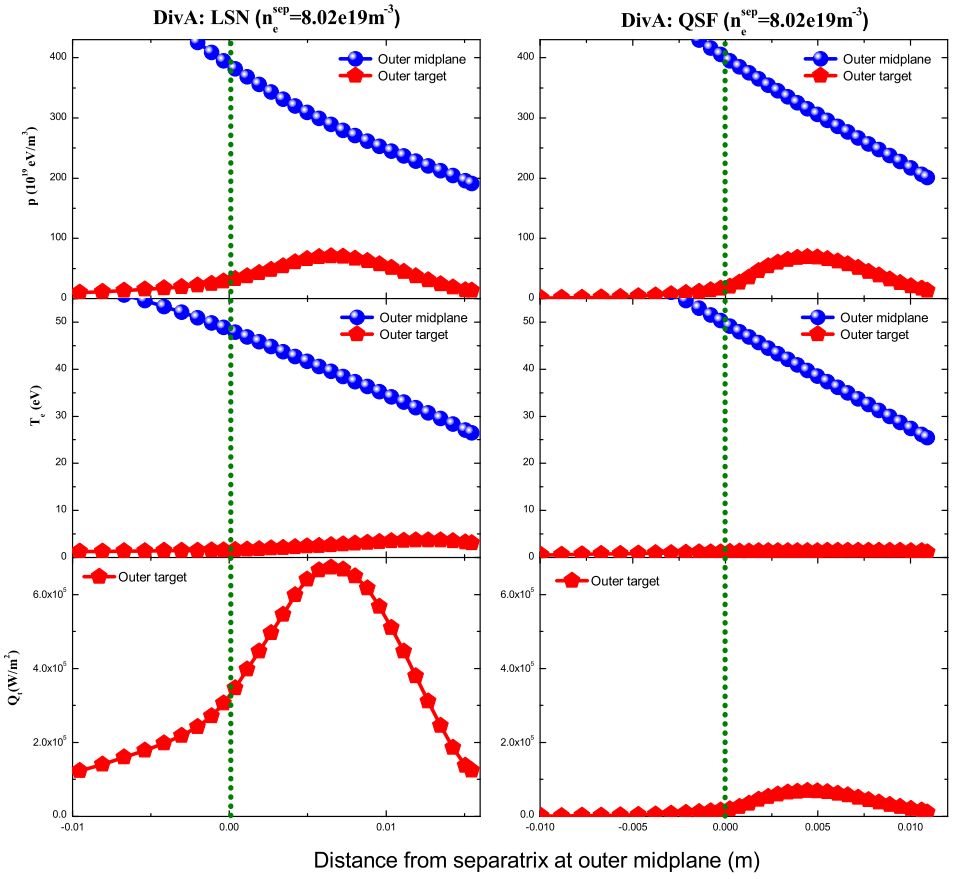

FIG. 6. The radial profiles of total pressure, electron temperature for the upstream and lower outer target, as well as the heat flux at lower outer target, versus the distance from the separatrix, mapped to the outer midplane, for both different EAST LSN and QSF divertor configurations with $n_e^{sep} = 8.02 \times 10^{19}\,\mathrm{m}^{-3}$.

lines. However, the divertor plasma temperature is significantly reduced. The low divertor plasma temperature is highly desirable, which can reduce impurity production and hence the erosion of divertor target plates. In addition, the conduction limited regime provides strong divertor screen for impurities. As shown in Fig. 5, the upstream-divertor pressure balance is maintained for both LSN and QSF divertor configurations with $n_e^{sep} = 1.6 \times 10^{19}\,\mathrm{m}^{-3}$. Compared with the behavior in the sheath limited regime, the divertor plasma temperature and heat flux along the lower outer target are dramatically reduced for both divertor configurations. As T_e is lowered down to 5 eV, the charge-exchange process between ions and neutrals becomes important, enhancing momentum and energy losses. When T_e is further reduced 1 eV, the volume recombination starts to play an important role, further reducing heat fluxes to the divertor target plates. The divertor detachment process is strongly dependent on neutral dynamics and atomic physics. The detached plasma regime is essential for steady state power exhaust. Fig. 6 shows the modelling results about the detached divertor plasma for LSN and QSF divertor configurations with $n_e^{sep} = 8.02 \times 10^{19}\,\mathrm{m}^{-3}$. As can be clearly seen, for LSN and QSF divertor configuration, there is a strong pressure drop at the divertor target, with a very low divertor plasma temperature, i.e., $T_e \approx 1$ eV. The corresponding heat load for both divertor configurations are also reduced to a very low level.

IV. SUMMARY

We have carried out detailed modeling of a new, QSF divertor configuration on EAST with SOLPS for different plasma regimes by varying the upstream plasma density, n_e^{sep}. The QSF divertor configuration significantly reduces the divertor heat flux, by a factor of 2–3, as a result of greater magnetic flux expansion, compared to LSN, at low upstream densities. As n_e^{sep} increases, QSF enables the divertor plasma to quickly move from the sheath-limited regime into the high recycling regime and achieves the detachment at a much lower upstream density than LSN. This indicates that QSF provides a promising means for the control of divertor heat flux at lower upstream density, which is highly desirable for current drive, thus facilitating long-pulse operations in EAST.

ACKNOWLEDGMENTS

The authors gratefully acknowledge the support from A. S. Kukushkin for generating the computational mesh for EAST QSF divertor configuration. All the numerical computations were performed at Shenma High Performance Computing Cluster at Institute of Plasma Physics, Chinese Academy of Sciences. This work was supported by National Magnetic Confinement Fusion Science Program of China under Contract Nos. 2015GB101000, 2014GB103000, 2014GB124006, 2013GB107003, and 2013GB107004; National Natural Science Foundation of China under Contract Nos. 11505234, 11347113, 11575235, 11422546, 11575236, 11575244, 11305216, and 11375010; Scientific Research Grant of Hefei Science Center of Chinese Academy of Sciences under Contract No. 2015SRG-HSC008; as well as the Thousand Talent Plan of China and Dean Foundation of Hefei Institutes of Physical Science Chinese Academy of Sciences.

[1]D. D. Ryutov, Phys. Plasmas **14**, 064502 (2007).
[2]D. D. Ryutov, R. H. Cohen, T. D. Rognlien, and M. V. Umansky, Phys. Plasmas **15**, 092501 (2008).
[3]F. Piras, S. Coda, I. Furno, J.-M. Moret, R. A. Pitts, O. Sauter, B. Tal, G. Turri, A. Bencze, B. P. Duval, F. Felici, A. Pochelon, and C. Zucca, Plasma Phys. Controlled Fusion **51**, 055009 (2009).
[4]V. A. Soukhanovskiia, J.-W. Ahn, R. E. Bell, D. A. Gates, S. Gerhardt, R. Kaita, E. Kolemen, H. W. Kugel, B. P. LeBlanc, R. Maingi, R. Maqueda, A. McLean, J. E. Menard, D. M. Mueller, S. F. Paul, R. Raman, A. L. Roquemore, D. D. Ryutov, and H. A. Scott, J. Nucl. Mater. **415**, S365–S368 (2011).
[5]D. D. Ryutov, R. H. Cohen, T. D. Rognlien, and M. V. Umansky, Plasma Phys. Controlled Fusion **54**, 124050 (2012).
[6]H. Reimerdes, G. P. Canal, B. P. Duval, B. Labit, T. Lunt, W. A. J. Vijvers, S. Coda, G. De Temmerman, T. W. Morgan, F. Nespoli, B. Tal, and TCV Team, Plasma Phys. Controlled Fusion **55**, 124027 (2013).
[7]R. Ambrosino, R. Albanese, S. Coda, M. Mattei, J.-M. Moret, and H. Reimerdes, Nucl. Fusion **54**, 123008 (2014).
[8]W. A. J. Vijvers, G. P. Canal, B. Labit, H. Reimerdes, B. Tal, S. Coda, G. C. De Temmerman, B. P. Duval, T. W. Morgan, J. J. Zielinski, and TCV Team, Nucl. Fusion **54**, 023009 (2014).
[9]M. Kotschenreuther, P. M. Valanju, and S. Mahajan, Bull. Am. Phys. Soc. **53**, 11 (2007).
[10]P. M. Valanju, M. Kotschenreuther, S. M. Mahajan, and J. Canik, Phys. Plasmas **16**, 056110 (2009).
[11]P. M. Valanju, M. Kotschenreuther, and S. M. Mahajan, Fusion Eng. Des. **85**(1), 46–52 (2010).
[12]M. Kotschenreuther, P. Valanju, S. Mahajan, L. J. Zheng, L. D. Pearlstein, R. H. Bulmer, J. Canik, and R. Maingi, Nucl. Fusion **50**, 035003 (2010).
[13]M. Kotschenreuther, P. M. Valanju, S. M. Mahajan, and J. C. Wiley, Phys. Plasmas **14**, 072502 (2007).
[14]M. Kotschenreuther, P. Valanju, B. Covele, and S. Mahajan, Phys. Plasmas **20**, 102507 (2013).
[15]B. Covele, P. Valanju, M. Kotschenreuther, and S. M. Mahajan, Nucl. Fusion **54**, 072006 (2014).
[16]Y. X. Wan, HT-7 Team, and HT-7U Team, Nucl. Fusion **40**, 1057 (2000).
[17]D. Normile, Science **312**, 992–993 (2006).
[18]B. N. Wan for the EAST and HT-7 Teams and International Collaborators, Nucl. Fusion **49**, 104011 (2009).
[19]H. Y. Guo, X. Gao, J. Li, G. N. Luo, S. Zhu, J. F. Chang, Y. P. Chen, W. Gao, X. Z. Gong, Q. S. Hua, Q. Li, S. C. Liu, T. F. Ming, J. Ou, Y. J. Shi, B. N. Wan, D. S. Wang, H. Q. Wang, J. Wang, Z. W. Wua, B. J. Xiao, Q. Xua, L. Zhang, and W. Zhang, J. Nucl. Mater. **415**, S369–S374 (2011).
[20]J. Li and B. N. Wan for the EAST Team and International Collaborators, Nucl. Fusion **51**, 094007 (2011).
[21]J. Li, H. Y. Guo, B. N. Wan, X. Z. Gong, Y. F. Liang, G. S. Xu, K. F. Gan, J. S. Hu, H. Q. Wang, L. Wang, L. Zeng, Y. P. Zhao, P. Denner, G. L. Jackson, A. Loarte, R. Maingi, J. E. Menard, M. Rack, and X. L. Zou, Nat. Phys. **9**, 817–821 (2013).
[22]H. Y. Guo, J. Li, X. Z. Gong, B. N. Wan, J. S. Hu, L. Wang, H. Q. Wang, J. E. Menard, M. A. Jaworski, K. F. Gan, S. C. Liu, G. S. Xu, S. Y. Ding, L. Q. Hu, Y. F. Liang, J. B. Liu, G. N. Luo, H. Si, D. S. Wang, Z. W. Wu, L. Y. Xiang, B. J. Xiao, L. Zhang, X. L. Zou, D. L. Hillis, A. Loarte, R. Maingi, and EAST Team, Nucl. Fusion **54**, 013002 (2014).
[23]H. Y. Guo, J. Li, B. N. Wan, X. Z. Gong, Y. F. Liang, G. S. Xu, X. D. Zhang, S. Y. Ding, K. F. Gan, J. S. Hu, L. Q. Hu, S. C. Liu, J. P. Qian, Y. W. Sun, H. Q. Wang, L. Wang, T. Y. Xia, B. J. Xiao, L. Zeng, Y. P. Zhao, P. Denner, J. R. Ferron, A. M. Garofalo, C. T. Holcomb, A. W. Hyatt, G. L. Jackson, A. Loarte, R. Maingi, J. E. Menard, M. Rack, W. M. Solomon, X. Q. Xu, M. Van Zeeland, X. L. Zou, and EAST Team, Phys. Plasmas **21**, 056107 (2014).
[24]G. Calabò, B. J. Xiao, S. L. Chen, Y. M. Duan, Y. Guo, J. G. Li, L. Liu, Z. P. Luo, L. Wang, J. Xu, B. Zhang, R. Albanese, R. Ambrosino, F. Crisanti, V. P. Ridolfini, F. Villone, B. Viola, L. Barbato, M. De Magistris, G. De Tommasi, E. Giovannozzi, S. Mastrostefano, S. Minucci, A. Pironti, G. Ramogida, A. A. Tuccillo, R. Zagórski, and EAST Team, Nucl. Fusion **55**, 083005 (2015).
[25]R. Schneider, D. Reiter, H. P. Zehrfeld, B. Braams, M. Baelmans, J. Geiger, H. Kastelewicz, J. Neuhauser, and R. Wunderlich, J. Nucl. Mater. **196–198**, 810–815 (1992).
[26]D. Reiter, J. Nucl. Mater. **196–198**, 80–89 (1992).
[27]A. S. Kukushkin and H. D. Pacher, Plasma Phys. Controlled Fusion **44**, 931 (2002).
[28]D. Coster, X. Bonnin, G. Corrigan, G. S. Kirnev, G. Mathews, and J. Spence, J. Nucl. Mater. **337–339**, 366–370 (2005).
[29]R. Schneider, X. Bonnin, K. Borrass, D. P. Coster, H. Kastelewicz, D. Reiter, V. A. Rozhansky, and B. J. Braams, Contrib. Plasma Phys. **46**, 3 (2006).
[30]A. V. Chankin, D. P. Coster, R. Dux, Ch. Fuchs, G. Haas, A. Herrmann, L. D. Horton, A. Kallenbach, M. Kaufmann, Ch. Konz, K. Lackner, C. Maggi, H. W. Müller, J. Neuhauser, R. Pugno, M. Reich, and W. Schneider, Plasma Phys. Controlled Fusion **48**, 839–868 (2006).
[31]G. D. Porter, S. Davies, B. LaBombard, A. Loarte, K. McCormick, R. Monk, M. Shimaka, and M. Sugihara, J. Nucl. Mater. **266–269**, 917–921 (1999).
[32]P. C. Stangeby, *The Plasma Boundary of Magnetic Fusion Devices* (IOP, Bristol, 2000).
[33]A. Guthrie and R. K. Wakerling, *The Characteristics of Electrical Discharges in Magnetic Fields* (McGraw-Hill, 1949), Chap. 3.